Letter

Analytic phase solution and point vortex model for dipolar quantum vortices

Ryan Doran [*]
Joint Quantum Centre (JQC) Durham–Newcastle, School of Mathematics, Statistics and Physics, Newcastle University, Newcastle upon Tyne NE1 7RU, United Kingdom and MARS: Mathematics for AI in Real-world Systems, School of Mathematical Sciences, Lancaster University, Lancaster LA1 4YF, United Kingdom

Thomas Bland [†]
Mathematical Physics, LTH, Lund University, Post Office Box 118, S-22100 Lund, Sweden

(Received 4 July 2025; revised 27 October 2025; accepted 9 October 2026; published 30 October 2026)

We derive an analytic expression for the phase of a quantum vortex in a dipolar Bose-Einstein condensate, capturing anisotropic effects from long-range dipole-dipole interactions. This solution provides a foundation for a dipolar point vortex model (DPVM), incorporating both phase-driven flow and dipolar forces. The DPVM reproduces key features of vortex pair dynamics seen in full simulations, including anisotropic velocities, deformed orbits, and directional motion, offering a minimal and accurate model for dipolar vortex dynamics. Our results open the door to analytic studies of vortices in dipolar quantum matter and establish a platform for exploring vortex dynamics and turbulence in these systems.

DOI: 10.1103/299h-xjc4

Circulating flow structures, or vortices, are central to the dynamics of both classical and quantum fluids. In systems governed by quantum coherence, such as superfluids and superconductors, vortices arise not as turbulent eddies but as topological singularities in the phase of a complex order parameter. Around each vortex core, the phase winds by integer multiples of 2π, enforcing quantized circulation and constraining the velocity field to be irrotational except at isolated points [1]. These features make quantum vortices not only signatures of superfluidity and superconductivity, but also essential building blocks for understanding quantum turbulence [2–4], lattice formation [5–7], and long-range coherence in interacting many-body systems [8–10].

Quantum vortices have a fixed core size and quantized circulation, meaning that they can be effectively described as interacting point particles. The point vortex model (PVM) offers a numerically efficient framework for capturing the dynamics of well-separated vortices in an ideal two-dimensional (2D) fluid [11]. While originally developed for classical incompressible flows, the model proves remarkably accurate for superfluid systems. The PVM has successfully described vortex dynamics in superfluid He [12], superfluid Fermi gases [13,14], and atomic Bose-Einstein condensates (BECs) [15,16]. This has led to a number of profound results in superfluid dynamics—from vortex-sound interaction [13] and vortex instabilities [14] to the enstrophy cascade [17] and the prediction [18] and experimental realization of large-scale flows [16] and Onsager vortex clustering [15]—as well as important results in classical turbulence [19,20] and statistical physics [21].

The key ingredient in the point vortex model is the *phase profile* of a single vortex. For fluids that interact only through isotropic short-range contact interactions, this phase has the simple analytic form $S(x, y) = \arctan(y/x)$ [22]. However, in certain classes of matter with anisotropic and long-range interactions—such as superconductors with Lifshitz invariants [23], polariton and coupled light-atom systems [24–26], and molecular [27] and dipolar quantum fluids—the interaction itself breaks radial symmetry. As such, despite extensive theoretical and numerical work no closed-form expression for the vortex phase exists to this day [28]. Without this, reduced models of vortex dynamics—so powerful in isotropic systems—have remained out of reach.

Vortices in dipolar BECs were observed only recently [29], made possible by the development of magnetostirring techniques that exploit the anisotropic dipolar interaction [30,31]. This experiment revealed striking vortex stripe lattices, a hallmark of anisotropic vortex-vortex interactions [30,32,33]. Several other theoretical predictions remain unconfirmed, including elliptically distorted vortex cores, roton-induced density oscillations around the core [31,33–40], and anisotropic vortex pair dynamics such as direction-dependent motion and suppressed annihilation [33,37,39,41].

In this Letter, we derive for the first time the phase profile of a quantum vortex in a dipolar condensate. Our analytic solution matches the numerically obtained phase with high accuracy and yields a self-consistent density ansatz for

[*]Contact author: r.doran@lancaster.ac.uk
[†]Contact author: thomas.bland@fysik.lu.se

Published by the American Physical Society under the terms of the Creative Commons Attribution 4.0 International license. Further distribution of this work must maintain attribution to the author(s) and the published article's title, journal citation, and DOI.

the vortex core. With the analytic phase, we formulate the dipolar point vortex model (DPVM), a minimal model that incorporates anisotropic phase-driven flow and long-range dipole-dipole interaction between vortices [42]. The DPVM is rigorously benchmarked against mean-field simulations of vortex pair dynamics, reproducing key features such as elliptic vortex-vortex orbits and directionally dependent motion of vortex-antivortex pairs [33,37,39,41]. Beyond dipolar condensates, our approach provides a general framework for treating vortices with anisotropic cores.

Deriving the dipolar vortex phase. In an infinite, homogeneous two-dimensional system, the phase $S(\rho, \vartheta)$ of a vortex with density $n(\rho, \vartheta)$ in an irrotational BEC must satisfy the continuity equation [22,43,44]

$$\frac{\partial n}{\partial t} + \nabla \cdot (n \nabla S) = 0. \tag{1}$$

Assuming the phase is independent of radius, $\rho = \sqrt{x^2 + y^2}$, and the density is independent of the azimuthal angle, $\vartheta = \arctan(y/x)$, Eq. (1) reduces trivially to $\partial^2 S(\vartheta)/\partial \vartheta^2 = 0$, which has solution $S(\vartheta) = q\vartheta$, where $q \in \mathbb{Z}$ is the topological charge of the vortex [22]. The second constant of integration is a phase shift that can be set to zero. This procedure is exact for any superfluid satisfying these assumptions, up to the singularity at $\rho = 0$.

In dipolar systems, however, vortices are predicted to develop elliptic cores [31,33–39], accompanied by lobes of increased and depleted density extending away from the center, invalidating the assumptions above. This anisotropic structure arises when the polarization axis is tilted by an angle α relative to the vortex line (normal to the xy plane), resulting in magnetostriction [45]—a stretching of the vortex core along the direction of polarization. Exemplar dipolar vortex density and phase profiles are shown in Fig. 1, obtained as stationary solutions of the dipolar Gross-Pitaevskii equation (GPE), which will be discussed in detail later. When the polarization axis is normal to the plane ($\alpha = 0$), the dipoles form an azimuthally symmetric density ring around the core, and the phase is unchanged from the nondipolar result [Fig. 1(b)]. However, tilting the dipoles into the plane breaks the angular symmetry of the density. In the strongly dipolar case with maximum tilt angle $\alpha = \pi/2$, as shown in Fig. 1(c), the core width broadens along the polarization direction, while regions of high density are maintained perpendicular to it. Strikingly, the phase profile responds to this deformation by concentrating phase gradients—hence superfluid velocity—along the polarization axis, with diminished gradients perpendicular to it. This is seen clearly by examining the nonlinear phase at a fixed radius away from the core, as shown in Fig. 1(a).

To find the dipolar vortex phase, it is natural to search for solutions to Eq. (1) in a modified coordinate system. By making the scale transformation $y \to \lambda^{-1} y$, we can define a shear-polar coordinate system (ρ', ϑ'), where $x = \rho' \cos\vartheta'$ and $y = \lambda^{-1}\rho' \sin\vartheta'$. Circles in (ρ', ϑ') are ellipses in (ρ, ϑ); hence, $\lambda > 1$ parametrizes the ellipticity of the vortex core. This transformation precisely recovers the assumption $S(\rho', \vartheta') \equiv S(\vartheta')$. We make a further approximation that in this coordinate system the vortex density is independent of ϑ', which we expect to be true away from the roton-induced density oscillations. Carefully defining the

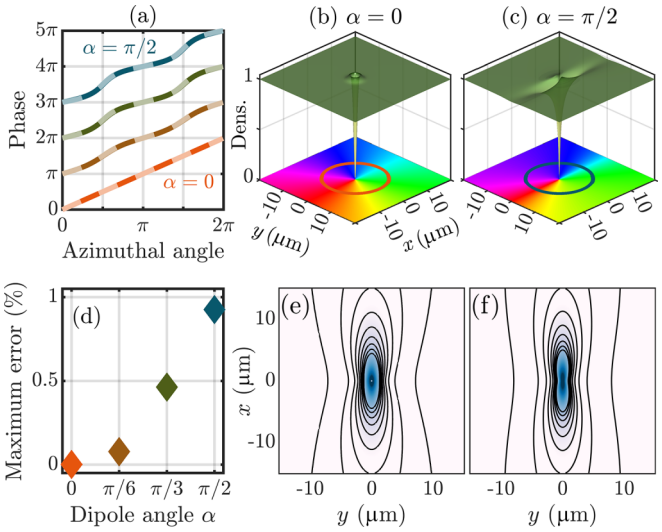


FIG. 1. Analytic phase of an elliptic vortex. (a) Solid lines show the vortex phase obtained from the dipolar GPE with interaction strength $\varepsilon_{dd} = 0.9$ at fixed radius $R = 10\,\mu$m; dashed lines indicate the corresponding solution to Eq. (3), using only the ellipticity λ_{FWMH} extracted from the full width at half maximum (FWHM) of the vortex density. The polarization angle α increases in steps of $\pi/6$, and each curve is vertically offset by π for clarity. (b), (c) Example solutions for the normalized vortex density $n(x, y)$ and phase at $\alpha = 0$ and $\alpha = \pi/2$, respectively. The colored circle marks the location from which the phase is extracted in panel (a). (d) Relative energy error: GPE vs vortex ansatz [Eq. (4) using λ_{opt}, solid], and GPE vs isotropic ansatz ($\lambda = 1$, dashed). Speed $|\nabla S|$ with $\alpha = \pi/2$ from (e) the GPE and (f) the analytic solution, with contours at steps of 20 μm/s. For reference, $\xi(0.9, 0) = 0.1\,\mu$m and $\xi(0.9, \pi/2) = 0.51\,\mu$m.

∇' operator in this coordinate system (see the Supplemental Material [46]), the stationary continuity equation is

$$(\nabla')^2 S = \frac{\partial}{\partial \vartheta'}\left[\sqrt{\frac{\tan^2\vartheta' + \lambda^2}{1 + \lambda^2 \tan^2\vartheta'}}\,\frac{\partial}{\partial \vartheta'}\right] S(\vartheta') = 0, \tag{2}$$

which is valid everywhere except at the origin. Remarkably, this equation is solvable and leads us to a solution for the phase. After integration and transformation back to Cartesian coordinates, we obtain

$$S(x, y) = q\Lambda\left\{(\lambda^2 - 1)F\left[\arctan\left(\frac{y}{x}\right)\middle|1 - \lambda^4\right] + \lambda^2 \Pi\left[1 - \lambda^2; \arctan\left(\frac{y}{x}\right)\middle|1 - \lambda^4\right]\right\}, \tag{3}$$

where $F(z|m)$ and $\Pi(n; z|m)$ are the incomplete elliptic integrals of the first and third kinds, respectively [47]. The integration constant is $\Lambda = \pi[4K(1 - \lambda^{-4}) - 2\lambda^{-2}\Pi(1 - \lambda^{-2}|1 - \lambda^{-4})]^{-1}$, where $K(m) \equiv F(\pi/2|m)$ and $\Pi(n|m) = \Pi(n; \pi/2\,|m)$ denote the corresponding complete first and third elliptic integrals. This choice ensures periodicity of the solution, $S|_{\vartheta=\pi} = S|_{\vartheta=-\pi}$. We can use this phase profile to approximate the form of the vortex density. We use our shear-polar coordinate system (ρ', ϑ') to modify the core profile in

Refs. [22,44], which leads to an ansatz profile for the vortex

$$\psi_v(x,y) = \sqrt{n_0}\frac{\sqrt{x^2+\lambda^2 y^2}}{\sqrt{x^2+\lambda^2 y^2+a^2}}e^{iS(x,y)}, \tag{4}$$

where n_0 is the background density of the fluid and a is a constant setting the core size.

To verify Eqs. (3) and (4), we introduce the governing equations for ultracold, weakly interacting, dilute dipolar quantum fluids. In a homogeneous magnetic field, interactions are described by the two-body pseudopotential $U(\mathbf{r}) = g\delta(\mathbf{r}) + \frac{3g_{\rm dd}}{4\pi}\frac{1-3\cos^2\theta}{|\mathbf{r}|^3}$ for particles of mass m, where θ is the angle between $\mathbf{r}$ and the polarization axis. The contact interaction $g = 4\pi\hbar^2 a_{\rm s}/m$ depends on the s-wave scattering length $a_{\rm s}$, tunable via Feshbach resonances [48], while the dipolar term $g_{\rm dd} = 4\pi\hbar^2 a_{\rm dd}/m$ is set by the dipolar length $a_{\rm dd}$. We define $\varepsilon_{\rm dd} = g_{\rm dd}/g$, noting instability for $\varepsilon_{\rm dd} \gtrsim 1$ [49].

In two dimensions, the full three-dimensional (3D) system is well approximated by the quasi-2D variational dipolar GPE [50], which has been applied across a range of dipolar systems [50–52]. In this model, the dynamics are governed by the dimensionally reduced wave function $\psi(\boldsymbol{\rho}, t)$, defined on the infinite plane $\boldsymbol{\rho} = (x, y)$, and the dipolar GPE takes the form

$$i\hbar\frac{\partial\psi}{\partial t} = \left[-\frac{\hbar^2\nabla^2}{2m} + \int \mathrm{d}^2\boldsymbol{\rho}'\, U_{\alpha,\sigma}(\boldsymbol{\rho}-\boldsymbol{\rho}')|\psi(\boldsymbol{\rho}')|^2\right]\psi, \tag{5}$$

where the modified interaction potential $U_{\alpha,\sigma}$ depends on the polarization angle α—with $\alpha = \pi/2$ corresponding to polarization along the x axis—and on the variational width σ in the tightly confined z direction (see the Supplemental Material [46]). Such a system has a chemical potential $\mu(\varepsilon_{\rm dd}, \alpha) = gn_{\rm 2D}[1 + \varepsilon_{\rm dd}(3\cos^2\alpha - 1)]$ [33,53,54] and healing length $\xi(\varepsilon_{\rm dd}, \alpha) = \hbar/\sqrt{m\mu}$, which determines the vortex core size. We choose an areal number density $n_{\rm 2D} = 500\,\mu\mathrm{m}^{-2}$ and fix the transverse harmonic confinement $\omega_z = 2\pi \times 167\,\mathrm{Hz}$, which are experimentally feasible parameters for ^{164}Dy where $\xi(0.9, 0) = 0.1\,\mu\mathrm{m}$, $\xi(0.9, \pi/2) = 0.51\,\mu\mathrm{m}$, and $\xi(\varepsilon_{\rm dd} = 0) = 0.16\,\mu\mathrm{m}$.

Figure 1 shows the results of the phase and total energy comparison. Solving Eq. (5) in imaginary time with an initial phase $S = \arctan(y/x)$, we recover the expected elliptic vortex cores for $\alpha \neq 0$ along with corresponding modifications to the phase profile. We extract the ellipticity directly from the density by measuring the square root of the ratio of the full width at half maximum along the x and y directions, obtaining $\lambda_{\rm FWHM} = [1,\ 1.27,\ 1.54,\ 1.76]$ for $\alpha = \pi[0,\ 1/6,\ 1/3,\ 1/2]$. Using these values of λ as the sole input to Eq. (3), we compute the dashed lines shown in Fig. 1(a), which show exceptional agreement with the numerically obtained phase. The largest deviation occurs for $\alpha = \pi/2$, where the density is no longer uniform at $R = 10\,\mu\mathrm{m}$, and the relative phase error reaches 2%. We have chosen the FWHM-derived value of λ to highlight our model as an experimentally accessible method for inferring the phase profile. However, by fitting Eq. (3) to the GPE phase, we obtain optimal values that reduce the error to below 1% for all α, namely, $\lambda_{\rm opt} = [1,\ 1.28,\ 1.64,\ 1.98]$ for the parameters considered. This is illustrated in Fig. 1(d), where using the same λ in both the density and phase ansatz yields a significantly lower relative error in the total vortex energy (over our computational grid) compared to the standard isotropic ansatz. Note that the error can be further reduced by considering a smaller value of $\varepsilon_{\rm dd}$. Finally, we compare the velocity fields generated by both methods in Figs. 1(e) and 1(f). Close to the core, Eq. (3) overestimates the anisotropy, which is also where the density modulations deviate most from a simple ellipse. In the Supplemental Material [46], we discuss the implications of taking $\lambda(\rho)$.

The point vortex model. Having an analytic form that closely matches the phase of an elliptic vortex unlocks the ability to derive a point vortex model for this system. Typically, the point vortex model can be derived from the phase of the system [55]; however, as this system is subject to anisotropic long-range interactions, it is also necessary to consider the vortex cores, which, as an absence of dipolar fluid, act as dipoles themselves. Where the intervortex spacing is greater than the healing length [56] and the fluid density is uniform away from the vortex core [55], the velocity contributions to the point vortex model can be decomposed as $\dot{\mathbf{r}}_j = \mathbf{v}_j^{(\rm P)} + \mathbf{v}_j^{(\rm DD)}$, where $\dot{\mathbf{r}}_j$ is the velocity of the jth vortex. The typical point vortex velocity term is proportional to the gradient of the phase, $\mathbf{v}_j^{(\rm P)} = \frac{\hbar}{m}\nabla S|_{\mathbf{r}_j}$, while the contribution from the dipole-dipole potential is $\mathbf{v}_j^{(\rm DD)} = q_j(2\pi\hbar n_{2D})^{-1}\hat{\mathbf{z}} \times \nabla V_{\rm DD}|_{\mathbf{r}_j}$, which is the perpendicular Peach-Koehler term arising from a force acting on the vortex [57]. For analytic simplicity, we take the 3D dipolar potential and set $z = 0$, giving

$$V_{\rm DD}(\boldsymbol{\rho}) = \frac{\hbar^2}{m}\frac{\xi_v\varepsilon_{\rm dd}}{\rho^3}\left(1 - 3\sin^2\alpha\frac{x^2}{\rho^2}\right), \tag{6}$$

where the core size ξ_v accounts for the atoms displaced from the vortex core [58]. From the derivatives of Eqs. (3) and (6), we can write the velocity contributions to the dipolar point vortex model as

$$\mathbf{v}_j^{(\rm P)} = \frac{\hbar\Lambda}{m}\sum_{\substack{k=1\\k\neq j}}^{N_v}\frac{q_k}{r_{jk}}\frac{\lambda^4 y_{jk}^2 + x_{jk}^2(2\lambda^2-1)}{(x_{jk}^2+\lambda^2 y_{jk}^2)\sqrt{x_{jk}^2+\lambda^4 y_{jk}^2}}\begin{pmatrix}-y_{jk}\\ x_{jk}\end{pmatrix}, \tag{7}$$

$$\mathbf{v}_j^{(\rm DD)} = \frac{3\hbar\xi_v\varepsilon_{\rm dd}q_j}{2\pi m n_{2D}}\sum_{\substack{k=1\\k\neq j}}^{N_v}\frac{1}{r_{jk}^7}\left\{[5x_{jk}^2\sin^2\alpha - r_{jk}^2]\begin{pmatrix}-y_{jk}\\ x_{jk}\end{pmatrix} - 2\sin^2\alpha\, r_{jk}^2\begin{pmatrix}0\\ x_{jk}\end{pmatrix}\right\}, \tag{8}$$

where $x_{jk} = x_j - x_k$, $y_{jk} = y_j - y_k$, and $r_{jk}^2 = x_{jk}^2 + y_{jk}^2$. These expressions clearly reduce to the standard PVM in the nondipolar limit, $\lambda = 1$ and $\varepsilon_{\rm dd} = 0$.

Vortex pair dynamics. With the model in hand, we investigate whether it can capture vortex pair phenomena in dipolar gases. Previous theoretical studies have predicted rich dynamics in such systems, including oval and dumbbell-shaped orbits for vortex-vortex pairs, as well as directionally dependent motion for vortex-antivortex pairs [28,33,37,39,41].

In Fig. 2, we present results for both models. We first focus on well-separated vortices separated by $10\,\mu\mathrm{m}$ that follow near-circular trajectories even in the presence of dipolar interactions. Despite the apparent similarity to the nondipolar case,

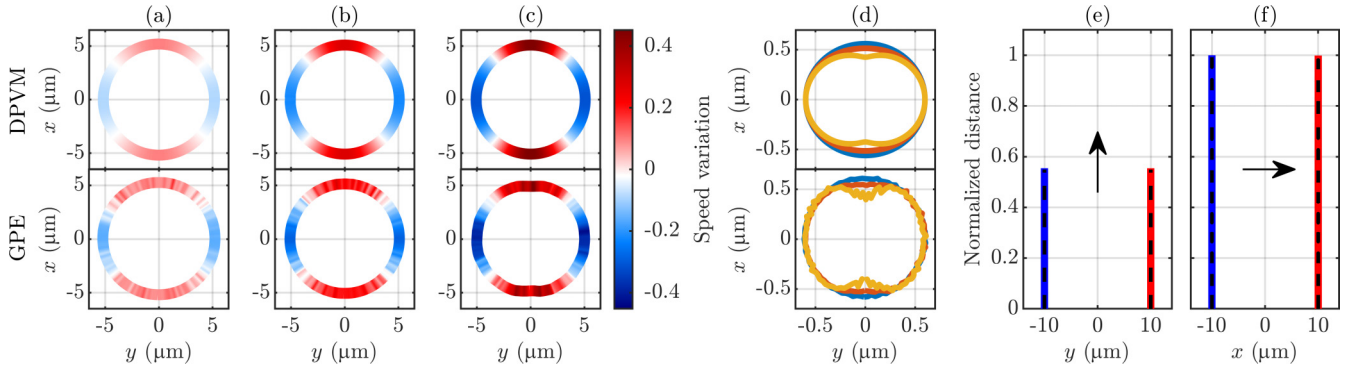


FIG. 2. Comparison of vortex pair dynamics. Vortex-vortex orbits with initial condition $x_j = 0$ and $y_1 = -y_2 = 5\,\mu$m in the DPVM (top row) and GPE (bottom row) for $\varepsilon_{dd} = 0.9$ and (a) $(\alpha, \lambda_{opt}) = (\pi/6, 1.08)$, (b) $(\pi/3, 1.15)$, and (c) $(\pi/2, 1.3)$. Color represents relative deviation from the local speed to the average speed v, i.e., $(|\mathbf{v}(x, y)| - v)/v$. (d) Same as panels (a)–(c) with $y_1 = -y_2 = 0.6\,\mu$m, with fixed $\alpha = \pi/2$ and $(\varepsilon_{dd}, \lambda_{opt}) = (0.3, 1.03)$, (0.6,1.08), (0.9,1.15). Traveling vortex-antivortex pairs with the vector between them (e) perpendicular and (f) parallel to the magnetic field and $(\varepsilon_{dd}, \alpha, \lambda_{opt}) = (0.9, \pi/2, 1.3)$. The DPVM vortex (blue, $q = 1$) and antivortex (red, $q = -1$) are shown with the corresponding GPE solutions (black dashed lines) overlaid, normalized to the same maximum traveled distance in panel (f). We fix $\xi_v = 20.3 a_{dd}$ throughout. For reference, $\xi(0.9, \pi/6) = 0.11\,\mu$m, $\xi(0.9, \pi/3) = 0.18\,\mu$m, $\xi(0.9, \pi/2) = 0.51\,\mu$m, $\xi(0.3, \pi/2) = 0.19\,\mu$m, and $\xi(0.6, \pi/6) = 0.25\,\mu$m.

the vortex motion is not uniform: The speed peaks when the pair is aligned head-to-tail with the magnetic field direction, and slows down when oriented perpendicular to it. To our knowledge, this anisotropic speed variation for well-separated dipolar vortices has not been discussed in detail beyond its connection to the anisotropic speed of sound [28,33] and provides a directly testable signature of anisotropic vortex dynamics.

To quantify this effect, we plot the instantaneous speed of one vortex along its orbit for increasing magnetic field tilt angles [Figs. 2(a)–2(c)]. The input value, λ_{opt}, is obtained by matching the total velocity field from the GPE ground state to $S(\boldsymbol{\rho} - \boldsymbol{\rho}_1) + S(\boldsymbol{\rho} - \boldsymbol{\rho}_2)$, with S given by Eq. (3). The DPVM captures the angular variation in speed with striking accuracy, exhibiting stronger modulation as the interaction anisotropy increases. As such, our model correctly describes the dominant anisotropic dynamics, while the minimal deviations from the GPE can be attributed to vortex-sound coupling that is absent in reduced models. We note that the velocity anisotropy is dominated by the phase contribution [Eq. (7)].

Dipolar vortices also exhibit qualitatively distinct orbital shapes. To explore this, we initialize the vortices in close proximity at positions $(0, \pm 0.6)\,\mu$m. Inspired by Fig. 3(a) of Ref. [39], we fix the dipole tilt angle and instead vary the scattering length, thereby tuning the relative dipolar interaction strength ε_{dd}, as shown in Fig. 2(d). The DPVM again closely reproduces the GPE trajectories, with noticeable deviations appearing only at $\varepsilon_{dd} = 0.9$, where overlapping density ripples around each vortex push the orbit back toward a circular shape away from head-to-tail configuration. The level of agreement at this short-range scale is especially noteworthy: Despite the highly inhomogeneous density in this regime, the essential physics is still accurately captured by the model. In contrast to the velocity modulation discussed above, this orbital deformation is driven by the dipolar interaction term [Eq. (8)], highlighting the necessity of its inclusion, as the dipole-dipole interactions fundamentally reshapes the nature of the vortex.

Finally, vortex-antivortex pairs are known to travel perpendicular to their separation vector, and in dipolar condensates this propagation speed additionally depends on the angle between the pair and the magnetic field axis [28]. In Figs. 2(e) and 2(f), we show that the DPVM captures this anisotropic propagation with high accuracy, matching the net traveled distance to within 1% of the GPE result. The agreement between our DPVM and the GPE results confirms the validity of our model.

Multivortex anisotropic orbits. An ideal application of the DPVM is the prediction of entirely new classes of stable orbits for N-vortex systems. In nondipolar superfluids, such dynamics have intrigued physicists since Helmholtz's seminal work on vortex motion [11,59]. The canonical example is that of three equally spaced vortices, which form a rigidly rotating triangle—an elegant solution derived analytically by Kirchhoff over two centuries ago [60]. In dipolar systems, however, this symmetry is broken by anisotropic interactions.

Figure 3 illustrates a strikingly altered three-vortex orbit. Each vortex now traces a bounded, quasiperiodic path, confined to a torus in phase space. Over time, these paths densely fill out a smooth oval envelope, shown in Fig. 3(a), with no exact repetition. Remarkably, despite the finite core size and density ripples in the full GPE dynamics, the DPVM reproduces the essential features of this motion with high fidelity, as shown in Fig. 3(b). Deviations only arise in regions of strong core-core interactions, where vortex-induced density ripples begin to interfere.

Conclusions. We have derived, for the first time, an analytic expression for the phase profile of a single vortex in a dipolar Bose-Einstein condensate by solving the continuity equation in a sheared polar coordinate system. This solution closely matches the phase obtained from mean-field simulations, even in the presence of anisotropy and roton-induced modulations. With the analytic phase in hand, we formulated the dipolar point vortex model (DPVM), which incorporates both anisotropic phase gradients and long-range dipole-dipole interactions, thereby providing a minimal predictive

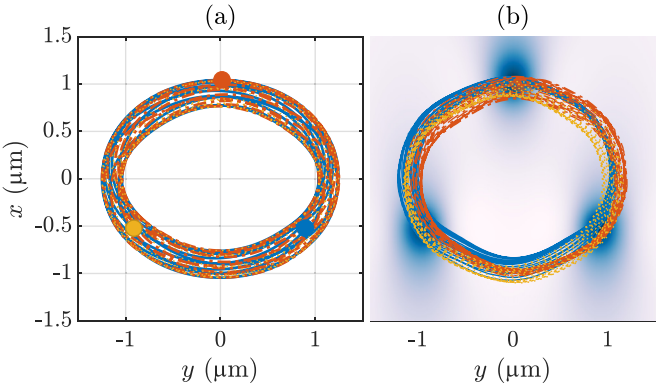


FIG. 3. Elliptic orbits of three vortices. Vortices are initially placed at the vertices of an equilateral triangle with circumradius 1 and evolved using (a) the DPVM and (b) the GPE. Vortex trajectories are color and line styled as follows: blue, solid; red, dashed; yellow, dotted. Initial vortex positions are marked in panel (a), while the background in panel (b) shows the initial condensate density. Parameters: $\alpha = \pi/2$, $\varepsilon_{\rm dd} = 0.6$, $\lambda_{\rm opt} = 1.16$, and others match Fig. 1; for reference, $\xi(0.6, \pi/2) = 0.25\,\mu$m.

framework for anisotropic vortex motion. The DPVM accurately captures vortex-vortex and vortex-antivortex dynamics seen in full Gross-Pitaevskii simulations, including elliptic orbits and direction-dependent motion. This reduced order model reveals how anisotropic phase gradients and dipole-dipole interactions independently reshape the governing vortex dynamics.

Our method is general and interaction-agnostic, providing a transferrable analytic framework for systems featuring elliptic vortex/fluxon cores [23–27]. The framework also extends to any inhomogeneous quantum fluid, provided a coordinate transformation renders the continuity equation solvable. Our model enables the efficient simulation of large vortex ensembles—beyond current computational limits [61–63]—where the resulting turbulence is anisotropic, leading to modifications in the vortex decay rate and energy cascade, and enabling the exploration of new stable N-vortex configurations in dipolar condensates. More broadly, our research demonstrates that quantized vortices can encode interaction anisotropy, opening an avenue for analytic and numerical vortex theory across a range of fluid systems.

Acknowledgments. We acknowledge stimulating discussions with Nick Parker at the inception of this work and thank Andy Martin for fruitful discussions throughout its development. R.D. is grateful to Stephanie Reimann for hospitality at Lund University. This work was supported by Research England under the Expanding Excellence in England (E3) funding stream, which was awarded to MARS: Mathematics for AI in Real-world Systems in the School of Mathematical Sciences at Lancaster University. R.D. was supported by the U.K. Engineering and Physical Sciences Research Council, Grant No. EP/X028518/1; T.B. was supported by the Knut and Alice Wallenberg Foundation (Grant No. KAW 2018.0217) and the Swedish Research Council (Grant No. 2022-03654VR).

Data availability. The data that support the findings of this article are not publicly available. The data are available from the authors upon reasonable request.

[1] R. Feynman, Application of quantum mechanics to liquid helium, in *Progress in Low Temperature Physics*, edited by C.J. Gorter (Elsevier, North-Holland, Amsterdam, 1955), Chap. II, pp. 17–53.

[2] E. A. L. Henn, J. A. Seman, G. Roati, K. M. F. Magalhães, and V. S. Bagnato, Emergence of turbulence in an oscillating Bose-Einstein condensate, Phys. Rev. Lett. **103**, 045301 (2009).

[3] M. C. Tsatsos, P. E. Tavares, A. Cidrim, A. R. Fritsch, M. A. Caracanhas, F. E. A. dos Santos, C. F. Barenghi, and V. S. Bagnato, Quantum turbulence in trapped atomic Bose–Einstein condensates, Phys. Rep. **622**, 1 (2016).

[4] L. Madeira, M. A. Caracanhas, F. dos Santos, and V. S. Bagnato, Quantum turbulence in quantum gases, Annu. Rev. Condens. Matter Phys. **11**, 37 (2020).

[5] A. A. Abrikosov, Nobel lecture: Type-II superconductors and the vortex lattice, Rev. Mod. Phys. **76**, 975 (2004).

[6] J. R. Abo-Shaeer, C. Raman, J. M. Vogels, and W. Ketterle, Observation of vortex lattices in Bose-Einstein condensates, Science **292**, 476 (2001).

[7] A. L. Fetter, Rotating trapped Bose-Einstein condensates, Rev. Mod. Phys. **81**, 647 (2009).

[8] M. W. Zwierlein, J. R. Abo-Shaeer, A. Schirotzek, C. H. Schunck, and W. Ketterle, Vortices and superfluidity in a strongly interacting Fermi gas, Nature (London) **435**, 1047 (2005).

[9] E. Casotti, E. Poli, L. Klaus, A. Litvinov, C. Ulm, C. Politi, M. J. Mark, T. Bland, and F. Ferlaino, Observation of vortices in a dipolar supersolid, Nature (London) **635**, 327 (2024).

[10] E. Poli, A. Litvinov, E. Casotti, C. Ulm, L. Klaus, M. J. Mark, G. Lamporesi, T. Bland, and F. Ferlaino, Synchronization in rotating supersolids, Nat. Phys. **21**, 1820 (2025).

[11] H. Helmholtz, Über Integrale der hydrodynamischen Gleichungen, welche den Wirbelbewegungen entsprechen, J. Reine Angew. Math. **55**, 25 (1858) [P. G. Tait, LXIII. On integrals of the hydrodynamical equations, which express vortex-motion, J. Science **33**, 485 (1867)].

[12] Y. P. Sachkou, C. G. Baker, G. I. Harris, O. R. Stockdale, S. Forstner, M. T. Reeves, X. He, D. L. McAuslan, A. S. Bradley, M. J. Davis, and W. P. Bowen, Coherent vortex dynamics in a strongly interacting superfluid on a silicon chip, Science **366**, 1480 (2019).

[13] W. Kwon, G. Del Pace, K. Xhani, L. Galantucci, A. Muzi Falconi, M. Inguscio, F. Scazza, and G. Roati, Sound emission and annihilations in a programmable quantum vortex collider, Nature (London) **600**, 64 (2021).

[14] D. Hernández-Rajkov, N. Grani, F. Scazza, G. Del Pace, W. J. Kwon, M. Inguscio, K. Xhani, C. Fort, M. Modugno, F. Marino, and G. Roati, Connecting shear flow and vortex array instabilities in annular atomic superfluids, Nat. Phys. **20**, 939 (2024).

[15] G. Gauthier, M. T. Reeves, X. Yu, A. S. Bradley, M. A. Baker, T. A. Bell, H. Rubinsztein-Dunlop, M. J. Davis, and T. W. Neely, Giant vortex clusters in a two-dimensional quantum fluid, Science **364**, 1264 (2019).

[16] M. T. Reeves, K. Goddard-Lee, G. Gauthier, O. R. Stockdale, H. Salman, T. Edmonds, X. Yu, A. S. Bradley, M. Baker, H. Rubinsztein-Dunlop, M. J. Davis, and T. W. Neely, Turbulent relaxation to equilibrium in a two-dimensional quantum vortex gas, Phys. Rev. X **12**, 011031 (2022).

[17] M. T. Reeves, T. P. Billam, X. Yu, and A. S. Bradley, Enstrophy cascade in decaying two-dimensional quantum turbulence, Phys. Rev. Lett. **119**, 184502 (2017).

[18] T. P. Billam, M. T. Reeves, B. P. Anderson, and A. S. Bradley, Onsager-Kraichnan condensation in decaying two-dimensional quantum turbulence, Phys. Rev. Lett. **112**, 145301 (2014).

[19] R. H. Kraichnan and D. Montgomery, Two-dimensional turbulence, Rep. Prog. Phys. **43**, 547 (1980).

[20] G. Boffetta and R. E. Ecke, Two-dimensional turbulence, Annu. Rev. Fluid Mech. **44**, 427 (2012).

[21] D. Montgomery and G. Joyce, Statistical mechanics of "negative temperature" states, Phys. Fluids **17**, 1139 (1974).

[22] A. L. Fetter, Vortices in an imperfect Bose gas. I. The condensate, Phys. Rev. **138**, A429 (1965).

[23] L. Fuchs, D. Kochan, J. Schmidt, N. Hüttner, C. Baumgartner, S. Reinhardt, S. Gronin, G. C. Gardner, T. Lindemann, M. J. Manfra, C. Strunk, and N. Paradiso, Anisotropic vortex squeezing in synthetic Rashba superconductors: A manifestation of Lifshitz invariants, Phys. Rev. X **12**, 041020 (2022).

[24] J. Léonard, A. Morales, P. Zupancic, T. Esslinger, and T. Donner, Supersolid formation in a quantum gas breaking a continuous translational symmetry, Nature (London) **543**, 87 (2017).

[25] J.-R. Li, J. Lee, W. Huang, S. Burchesky, B. Shteynas, F. Ç. Top, A. O. Jamison, and W. Ketterle, A stripe phase with supersolid properties in spin–orbit-coupled Bose–Einstein condensates, Nature (London) **543**, 91 (2017).

[26] N. Goldman, G. Juzeliūnas, P. Öhberg, and I. B. Spielman, Light-induced gauge fields for ultracold atoms, Rep. Prog. Phys. **77**, 126401 (2014).

[27] N. Bigagli, W. Yuan, S. Zhang, B. Bulatovic, T. Karman, I. Stevenson, and S. Will, Observation of Bose–Einstein condensation of dipolar molecules, Nature (London) **631**, 289 (2024).

[28] A. M. Martin, N. G. Marchant, D. H. J. O'Dell, and N. G. Parker, Vortices and vortex lattices in quantum ferrofluids, J. Phys.: Condens. Matter **29**, 103004 (2017).

[29] L. Klaus, T. Bland, E. Poli, C. Politi, G. Lamporesi, E. Casotti, R. N. Bisset, M. J. Mark, and F. Ferlaino, Observation of vortices and vortex stripes in a dipolar condensate, Nat. Phys. **18**, 1453 (2022).

[30] S. B. Prasad, T. Bland, B. C. Mulkerin, N. G. Parker, and A. M. Martin, Vortex lattice formation in dipolar Bose-Einstein condensates via rotation of the polarization, Phys. Rev. A **100**, 023625 (2019).

[31] T. Bland, G. Lamporesi, M. J. Mark, and F. Ferlaino, Vortices in dipolar Bose–Einstein condensates, C. R. Phys. **24**, 133 (2023).

[32] J. Zhang and H. Zhai, Vortex lattices in planar Bose-Einstein condensates with dipolar interactions, Phys. Rev. Lett. **95**, 200403 (2005).

[33] C. Ticknor, R. M. Wilson, and J. L. Bohn, Anisotropic superfluidity in a dipolar Bose gas, Phys. Rev. Lett. **106**, 065301 (2011).

[34] S. Yi and H. Pu, Vortex structures in dipolar condensates, Phys. Rev. A **73**, 061602(R) (2006).

[35] M. Jona-Lasinio, K. Łakomy, and L. Santos, Roton confinement in trapped dipolar Bose-Einstein condensates, Phys. Rev. A **88**, 013619 (2013).

[36] M. Jona-Lasinio, K. Łakomy, and L. Santos, Time-of-flight roton spectroscopy in dipolar Bose-Einstein condensates, Phys. Rev. A **88**, 025603 (2013).

[37] B. C. Mulkerin, R. M. W. van Bijnen, D. H. J. O'Dell, A. M. Martin, and N. G. Parker, Anisotropic and long-range vortex interactions in two-dimensional dipolar Bose gases, Phys. Rev. Lett. **111**, 170402 (2013).

[38] B. Mulkerin, D. O'Dell, A. Martin, and N. Parker, Vortices in the two-dimensional dipolar Bose gas, J. Phys.: Conf. Ser. **497**, 012025 (2014).

[39] S. B. Prasad, N. G. Parker, and A. W. Baggaley, Vortex-pair dynamics in three-dimensional homogeneous dipolar superfluids, Phys. Rev. A **109**, 063323 (2024).

[40] A. Villois, M. Onorato, and D. Proment, Vortex to rotons transition in dipolar Bose-Einstein condensates, Phys. Rev. Lett. **134**, 253401 (2025).

[41] S. Gautam, Dynamics of the corotating vortices in dipolar Bose–Einstein condensates in the presence of dissipation, J. Phys. B: At. Mol. Opt. Phys. **47**, 165301 (2014).

[42] We note here that throughout this work "dipole" refers to the long-range interaction, not to be confused with vortex dipoles, which we will refer to as vortex-antivortex pairs.

[43] N. G. Berloff, Padé approximations of solitary wave solutions of the Gross–Pitaevskii equation, J. Phys. A: Math. Gen. **37**, 1617 (2004).

[44] A. S. Bradley and B. P. Anderson, Energy spectra of vortex distributions in two-dimensional quantum turbulence, Phys. Rev. X **2**, 041001 (2012).

[45] N. Ekreem, A. Olabi, T. Prescott, A. Rafferty, and M. Hashmi, An overview of magnetostriction, its use and methods to measure these properties, J. Mater. Process. Technol. **191**, 96 (2007).

[46] See Supplemental Material at http://link.aps.org/supplemental/10.1103/299h-xjc4 for further details of the phase profile, the optimal value of λ, and our GPE numerics.

[47] M. Abramowitz and I. A. Stegun, *Handbook of Mathematical Functions with Formulas, Graphs, and Mathematical Tables* (Dover, New York, 1965).

[48] C. Chin, R. Grimm, P. Julienne, and E. Tiesinga, Feshbach resonances in ultracold gases, Rev. Mod. Phys. **82**, 1225 (2010).

[49] T. Lahaye, C. Menotti, L. Santos, M. Lewenstein, and T. Pfau, The physics of dipolar bosonic quantum gases, Rep. Prog. Phys. **72**, 126401 (2009).

[50] D. Baillie and P. B. Blakie, A general theory of flattened dipolar condensates, New J. Phys. **17**, 033028 (2015).

[51] B. T. E. Ripley, D. Baillie, and P. B. Blakie, Two-dimensional supersolidity in a planar dipolar Bose gas, Phys. Rev. A **108**, 053321 (2023).

[52] P. Senarath Yapa and T. Bland, Anomalous dispersion of shear waves in dipolar supersolids, Phys. Rev. A **112**, L021303 (2025).

[53] N. G. Parker and D. H. J. O'Dell, Thomas-Fermi versus one- and two-dimensional regimes of a trapped dipolar Bose-Einstein condensate, Phys. Rev. A **78**, 041601(R) (2008).

[54] Y. Cai, M. Rosenkranz, Z. Lei, and W. Bao, Mean-field regime of trapped dipolar Bose-Einstein condensates in one and two dimensions, Phys. Rev. A **82**, 043623 (2010).

[55] O. Törnkvist and E. Schröder, Vortex dynamics in dissipative systems, Phys. Rev. Lett. **78**, 1908 (1997).

[56] M. D. Bustamante and S. Nazarenko, Derivation of the Biot-Savart equation from the nonlinear Schrödinger equation, Phys. Rev. E **92**, 053019 (2015).

[57] M. Peach and J. S. Koehler, The forces exerted on dislocations and the stress fields produced by them, Phys. Rev. **80**, 436 (1950).

[58] We have verified that we can obtain the same results taking the real space form of the quasi-2D dipole-dipole interaction [54]; however, the final expressions are much longer, and the agreement between GPE and DPVM persists (not shown). In addition, we have verified that taking a regularization parameter Δ such that $\rho^3 \to (\rho^3 + \Delta)$ [64] does not affect our results, due to the fact that the vortices in our model are well separated, and Δ only becomes important close to the vortex core.

[59] H. Aref, Point vortex dynamics: A classical mathematics playground, J. Math. Phys. **48**, 065401 (2007).

[60] G. Kirchhoff, *Vorlesungen Über mathematische Physik*, 3rd ed. (Teubner, Leipzig, 1883), Vol. 1, p. 257.

[61] T. Bland, G. W. Stagg, L. Galantucci, A. W. Baggaley, and N. Parker, Quantum ferrofluid turbulence, Phys. Rev. Lett. **121**, 174501 (2018).

[62] S. Sabari, R. Kishor Kumar, and L. Tomio, Vortex dynamics and turbulence in dipolar Bose-Einstein condensates, Phys. Rev. A **109**, 023313 (2024).

[63] N. Rasch, L. Chomaz, and T. Gasenzer, Anomalous nonthermal fixed point in a quasi-two-dimensional dipolar Bose gas, Phys. Rev. A **112**, 053310 (2025).

[64] P. Molignini and B. Chakrabarti, Stability of dipolar bosons in a quasiperiodic potential, Phys. Rev. Res. **7**, 023237 (2025).